ACS APPLIED MATERIALS & INTERFACES

www.acsami.org
Research Article

Enhancing Interlayer Charge Transport of Two-Dimensional Perovskites by Structural Stabilization via Fluorine Substitution

Elizabeth Stippell, Wei Li, Claudio Quarti, David Beljonne, and Oleg V. Prezhdo*

Cite This: ACS Appl. Mater. Interfaces 2025, 17, 2032−2040
Read Online

ACCESS | Metrics & More | Article Recommendations

ABSTRACT: Two-dimensional lead-halide perovskites provide a more robust alternative to three-dimensional perovskites in solar energy and optoelectronic applications due to increased chemical stability afforded by interlayer ligands. At the same time, the ligands create barriers for interlayer charge transport, reducing device performance. Using a recently developed ab initio simulation methodology, we demonstrate that ligand fluorination can enhance both hole and electron mobility by 1−2 orders of magnitude. The simulations show that the enhancement arises primarily from improved structural order and reduced thermal atomic fluctuations in the system rather than increased interlayer electronic coupling. Arising from stronger hydrogen bonding and dipolar interactions, the higher structural stability decreases the reorganization energy that enters the Marcus formula and increases the charge transfer rate. The detailed atomistic insights into the electron and hole transfer in layered perovskites indicate that the use of interlayer ligands that make the overall structure more robust is beneficial simultaneously for chemical stability and charge transport, providing an important guideline for the design of new, efficient materials.

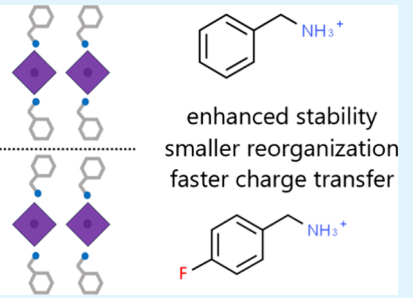

KEYWORDS: *metal halide perovskites, two-dimensional, Marcus theory, charge transport, reorganization energy, electron-vibrational interactions, solar energy, optoelectronics*

1. INTRODUCTION

Understanding charge transfer processes in two-dimensional (2D) perovskites is vital for their development and applications in optoelectronic and photochemical systems. Perovskites have been widely studied for applications in solar cell, light-emitting diodes, detectors, etc.[1−5] 2D perovskites, specifically, have gained interest over the past years due to their tunable bandgap and increased stability compared to their three-dimensional counterparts.[4] A 2D perovskite is made by inserting bulky organic spacers between singular inorganic crystalline layers. Lead-halide compounds constitute the most popular choice of crystals. 2D perovskites can be categorized into either Ruddlesden−Popper (RP) or Dion-Jacobson (DJ) perovskites, the former having a monovalent cation and the latter containing a divalent cation.[1]

The general formula for a 2D perovskite is $A_{n+1}B_nX_{3n+1}$, where A is the organic spacer, B is the cation in the perovskite crystal (lead), and X is the anion, e.g., iodine. The subscript variable n corresponds to the number of octahedral layers in the crystal. In the case of a 2D perovskite, n is a small integer. The general 2D perovskite formula may be rewritten to describe an RP perovskite, $A_2A'_{n-1}B_nX_{3n+1}$ where A' is the small, monovalent cation that resides between adjacent inorganic layers.[1] In the case of a single-layer crystalline structure, $n = 1$, there are no adjacent inorganic layers, and hence, no monovalent cations are present. Furthermore, for each lead−iodine polyhedron, there are two interacting organic spacers, represented by A.

Although 2D perovskites are more stable compared to their 3D counterparts, they trail behind in terms of power conversion efficiency (PCE) with recorded PCEs exceeding 18% and 25% for 2D perovskites[4] and 3D perovskites,[6] respectively.

The organic spacers act as insulators between the inorganic layers, helping to improve the stability of the structures but hindering the charge transfer processes by confining the charges to the inorganic layers and making out-of-plane charge transfer less efficient.[4] One of the most prominent challenges in designing efficient 2D perovskites is overcoming this isolation of charges in order to create systems that favor charge mobility. The goal can be achieved by tuning the properties of the organic spacers.[7]

The addition of fluorine in the organic spacers of 2D perovskites can be used to enhance charge mobility and hopping rates.[8,9] Fluorine is a good candidate to control the

Received: October 16, 2024
Revised: December 4, 2024
Accepted: December 10, 2024
Published: December 16, 2024

electronic properties of the perovskite due to its relatively small size and high electronegativity. The high electronegativity acts to withdraw charge density from the polyhedral-facing tail, inducing charge transfer away from the inorganic polyhedral and toward the adjacent organic spacer layer. It has been reported that the inclusion of fluorine in an organic spacer increases the dipole moment when placed opposite to that of the positive NH_3^+ group.[10,11] Fluorine is also reported to enhance and shorten hydrogen bonds, increasing orbital overlap and providing better opportunity for charge transfer to occur between layers.[11,12] The stronger hydrogen bond increases the electronic coupling between layers.

Various fluorinated organic spacers have been proposed, such as substituted phenethylammonium (PEA),[12,13] aromatic formamidine,[14] azetidine,[15] and PTMA,[16] to name a few researched spacers that have led to PCEs as high as 19%. One of such organic spacers is fluorinated benzylammonium (F-BZA) which contains a fluorine atom at the para-position of the benzene ring. In synthesizing this structure, fluorine slows crystal growth, allowing the system to align itself vertically therefore changing the orientation of the charge transport. The addition of the fluorine atom increases the PCE by 35% compared to the unsubstituted benzylammonium (BZA) based perovskite.[8]

Vertical (out-of-plane) transport, as reported in various 2D perovskites,[12,17−19] is relevant in photovoltaic applications. The out-of-plane charge transfer allows charges to travel across the organic spacers and therefore between layers.[20] The interlayer transport improves the photovoltaic and optoelectronic properties of the 2D perovskite.[21]

Boeije et al.[17] studied the significance of electronically active versus inactive spacers, in particular, comparing Cz-C_i and PEA molecules, respectively. The electronically active spacer increased the interlayer coupling and the out-of-plane charge mobility compared to its inert counterpart. Zhang et al.[12] studied the PEA spacer further, including a fluorinated version which improves charge transfer through optimizing the vertical electronic coupling between the crystal layers.

Theoretical investigations are a powerful tool in studying electronic structure, atomistic dynamics and quantum electronic dynamics at a molecular level. Various researchers have examined the electronic properties of 2D perovskites using density functional theory (DFT)[10,12] paired with experimental results, including measurements via scanning electron microscopy and conductive atomic force microscopy,[12] and current density−voltage ($J-V$) measurements.[8,22] There are few ab initio quantum dynamics studies of charge transfer in 2D perovskites,[18,23−29] indicating a need for more in-depth theoretical analyses to better understand the charge transport mechanisms in the 2D perovskites.

In this work, we report a detailed atomistic investigation of charge transfer processes in 2D perovskites. By applying the recently developed ab initio approach[18] combining the projection operator diabatization method, molecular dynamics simulations, and Marcus theory calculations, we demonstrate that fluorination of organic spacers simultaneously improves material stability and charge transport. Focusing on 2D lead−iodine perovskites containing either BZA or F-BZA organic spacers, we show that fluorination increases intermolecular interactions, including hydrogen bonding and dipole−dipole coupling, and make the material structure more robust overall. The decreased structural fluctuations in the fluorinated system reduce the reorganization energy that enters the Marcus theory expression, thereby increasing the charge transfer rate. While it is often assumed that fluorination increases the electronic coupling between layers, due to stronger ligand−ligand interactions and extended charge density, we find this to be an insignificant factor compared to changes in the reorganization energy. Fluorination enhances electron and hole mobility by 1−2 orders of magnitude, in agreement with the recent experimental studies.[8,30−32] The atomistic insights into the charge transport properties of 2D lead-halide perovskites provided by the current work generate important guidelines for the development of higher quality solar energy and optoelectronic materials. In particular, the results show that making the overall material structure more robust simultaneously improves chemical stability as well as charge and energy transport.

2. METHODS

2.1. Projection Operator Diabatization Method. The projection operator diabatization (POD) method was described by Kondov et al.[33] and can be used to calculate electronic couplings between diabatic states of various systems.[18,34−36] Currently, we apply the method to obtain the interlayer coupling in the BZA- and F-BZA-PbI_4 systems. The POD method uses the Kohn−Sham (KS) Hamiltonian matrix, $H(\mathbf{k})$, of a periodic system calculated self-consistently through the OpenMX software package.[37,38]

$$H(\mathbf{k}) = \sum_{\mathbf{n}} e^{i\mathbf{R_n}\mathbf{k}} \langle \phi_i(\mathbf{r}) | H | \phi_j(\mathbf{r} - \mathbf{R_n}) \rangle \tag{1}$$

Here, $e^{iR_n\mathbf{k}}$ is a phase factor term, $\mathbf{k}$ is the crystal momentum, $\mathbf{R_n}$ is the crystal lattice parameter, and ϕ_i represents the pseudoatomic orbitals at site i. The atomic basis functions consist of linearly independent and nonorthogonal functions which can be orthogonalized using the Löwdin method:[39,40]

$$\left|\tilde{\phi}_i\right\rangle = \sum_j S_{ji}^{-1/2} \left|\phi_j\right\rangle \tag{2}$$

where $S_{ji} = \langle \phi_j \mid \phi_i \rangle$ is the atomic orbital overlap. After the Löwdin orthogonalization, the generalized KS eigenproblem is transformed from

$$H_{KS}C = SCE \tag{3}$$

to

$$\tilde{H}\tilde{C} = \tilde{C}E \tag{4}$$

where

$$\tilde{C} = X^{-1}C \tag{5}$$

and $X^{-1} = S^{-1/2}$ is the transformation matrix. The KS Hamiltonian matrix transforms in the orthogonal basis into:

$$\tilde{H} = S^{-1/2} H S^{-1/2} \tag{6}$$

The system can then be separated into donor (D) and acceptor (A) fragments. Currently, each fragment has two $[PbI_6]^{-4}$ units and four corresponding organic spacer units, achieving charge neutrality, as visualized in Figures 1 and 2. Specific blocks in the KS matrix can be labeled as belonging to either D, or A, or D−A coupling:

$$\tilde{H} = \begin{bmatrix} \tilde{H}_{DD} & \tilde{H}_{DA} \\ \tilde{H}_{AD} & \tilde{H}_{AA} \end{bmatrix} \tag{7}$$

A unitary transformation matrix, $\tilde{C}_T$, can then be used to partially diagonalize the matrix, H':

https://doi.org/10.1021/acsami.4c17876
ACS Appl. Mater. Interfaces 2025, 17, 2032−2040

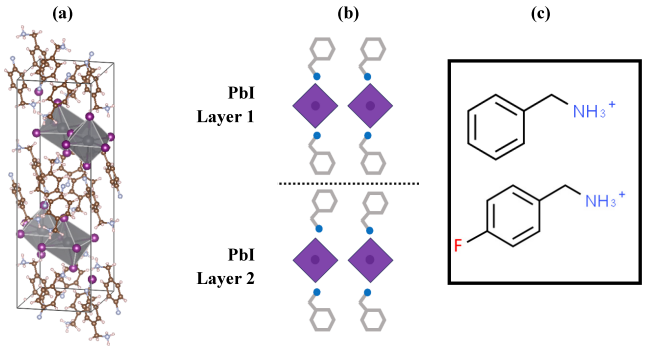

Figure 1. (a) Atomic structure of the 2D perovskite unit cell. (b) Schematic of the 2D perovskite systems, showing inorganic layers and organic spacers. (c) Chemical structure of the organic spacers for the BZA-PbI_4 and F-BZA-PbI_4 systems.

$$\tilde{C}_T = \begin{bmatrix} \tilde{C}_D & 0 \\ 0 & \tilde{C}_A \end{bmatrix} \tag{8}$$

$$H' = \tilde{C}_T^{+} H \tilde{C}_T \tag{9}$$

$$H' = \begin{bmatrix} \varepsilon_{1,D} & 0 & & & \\ 0 & \varepsilon_{2,D} & & V_{DA} & \\ \vdots & & \ddots & & \\ & & & \varepsilon_{1,A} & 0 \\ & V_{AD} & & 0 & \varepsilon_{2,A} \\ & & & \vdots & \ddots \end{bmatrix} \tag{10}$$

The diagonal blocks contain the orbital energies of the diabatic states, ε_D and ε_A, corresponding to the donor and acceptor states, respectively. The off-diagonal blocks contain the diabatic donor−acceptor couplings.

According to eq 1, the off-diagonal couplings are dependent on the momentum, **k**. This allows the use of arbitrary k-points in the calculations. It is feasible to focus only on the Γ-point, because both systems exhibit direct band gaps located at the Γ-point. The calculated band structure and projected density of states (DOS) are shown in Figure 3. This also simplifies the phase factor in eq 1 to 1.

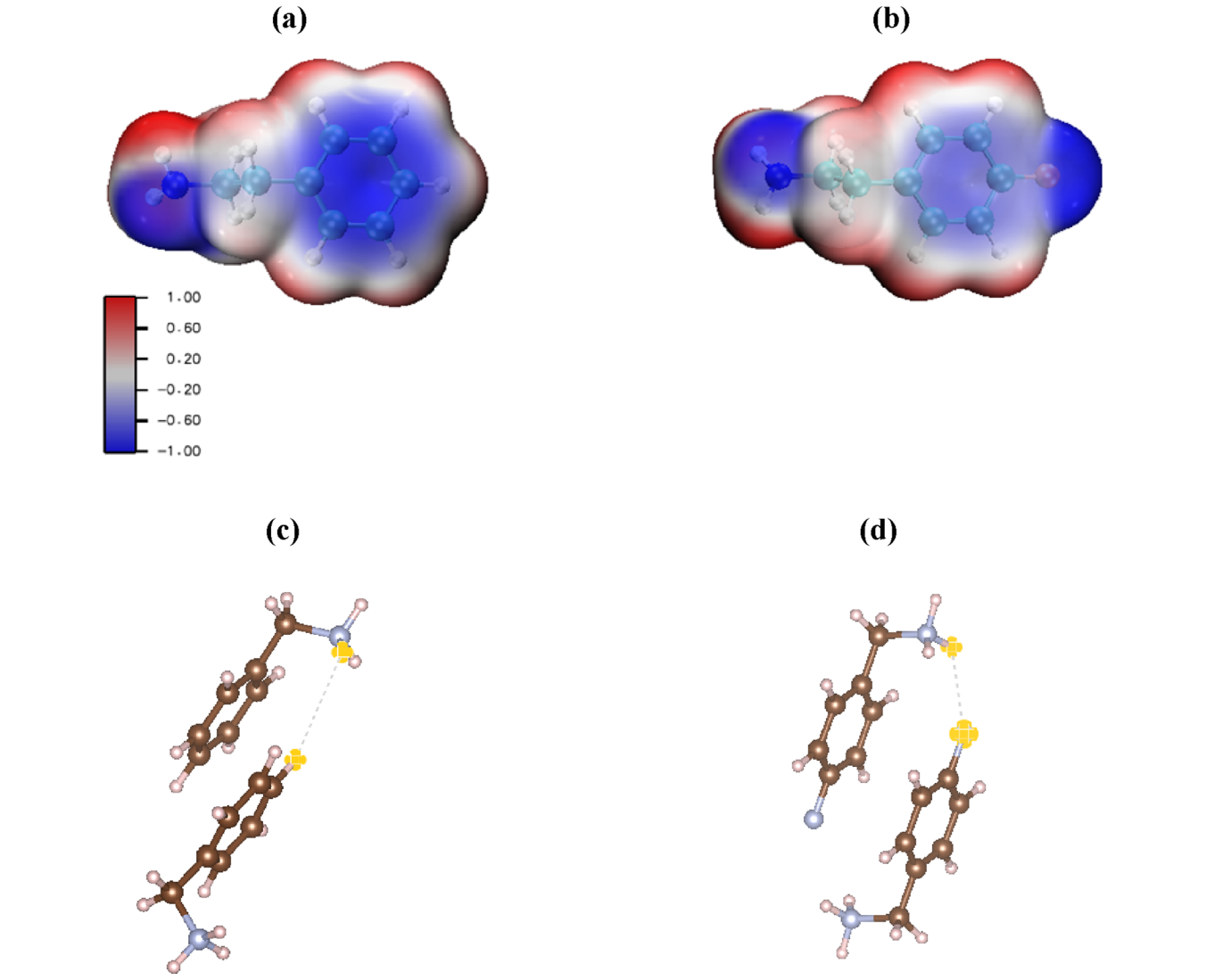

Figure 2. Electrostatic potentials in (a) BZA and (b) F-BZA organic spacers. Electron-rich areas are denoted in blue. The electron-rich area extends onto the F atom of F-BZA, while it is on the benzene ring in BZA. Geometry of adjacent (c) BZA and (d) F-BZA organic spacers from the two layers. The F-BZA spacers adjust to allow for N−H···F hydrogen bonding, part d.

https://doi.org/10.1021/acsami.4c17876
ACS Appl. Mater. Interfaces 2025, 17, 2032−2040

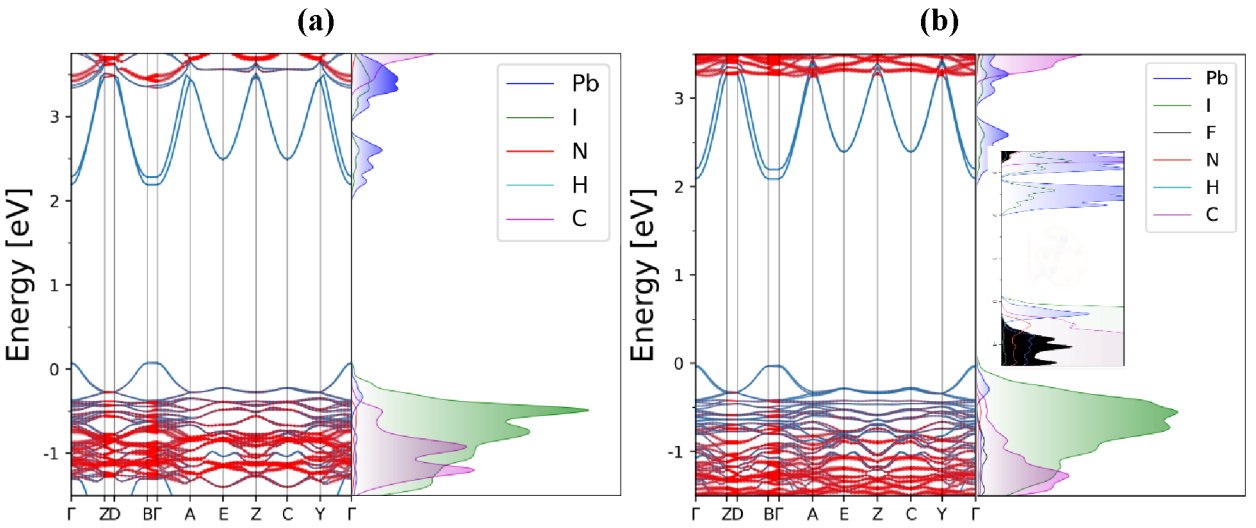

Figure 3. Band structure and projected density of states (pDOS) for (a) BZA-PbI_4 and (b) F-BZA-PbI_4. The red dots in the band structure indicate contribution of the organic spacers, with the larger dots corresponding to larger contribution. The inset in (b) shows magnified pDOS to highlight the contribution by fluorine (black).

2.2. Marcus Theory. The interlayer electronic couplings and diabatic state energies computed at each time step along the MD trajectories with the POD method can be used with the Marcus theory[41] to calculate the hole and electron transfer times as well as the charge carrier mobility. In the case of weak coupling and high temperature, the charge transfer rate can be represented in the Marcus theory as

$$k_{Marcus} = \left(\frac{V^2}{\hbar}\right)\sqrt{\frac{\pi}{\lambda k_B T}}\exp\left(-\frac{(\Delta G + \lambda)^2}{4\lambda k_B T}\right) \quad (11)$$

where V is the electronic donor−acceptor coupling, λ is the reorganization energy, ΔG is the Gibbs free energy of the electron transfer reaction, k_B is the Boltzmann constant (8.617×10^{-5} eV/K), and T is the temperature in Kelvin. The Gibbs free energy of reaction can be set to zero due to the crystal symmetry of the two layers, dictated by the *Pbca* space group.

The reorganization energy is obtained from phonon-induced fluctuations, σ, of the diabatic electronic energies of the two layers according to

$$\lambda = \frac{\sigma^2}{2k_B T} \quad (12)$$

where σ is defined as

$$\sigma = \langle (dE - \langle dE \rangle)^2 \rangle \quad (13)$$

Here, dE the difference between the diabatic electronic energies of layers 1 and 2. The reorganization energy can also be calculated using the spectral density, $J(\omega)$, as discussed in ref 18.

Once the Marcus rate is calculated, its inverse can be taken as the charge hopping time. This time scale can then be used to calculate the carrier mobility using the following equation:

$$\mu_{hopping} = \frac{eD}{k_B T} = \frac{ek_{Marcus}L^2}{k_B T} \quad (14)$$

Here, e is the charge of an electron, k_{Marcus} is the Marcus hopping rate, and L is the distance between the two layers' centers of mass.

2.3. Electronic Structure Calculations. Electronic structure calculations, geometry optimization and ab initio molecular dynamics (MD) were carried out using the Vienna *Ab initio* Simulation Package[42] (VASP). The Perdew−Burke−Ernzerhof[43] (PBE) DFT functional was employed. The van der Waals interactions were described with Grimme's DFT-D3 dispersion correction.[44] A plane-wave energy cutoff of 400 eV was used to ensure convergence with a 5 × 5 × 1 Monkhorst-pack k-point mesh.

The structures were first optimized. Then, the Nose-Hoover thermostat was used with a time step of 1 fs to increase the temperature of the systems from 0 to 300 K over a 3 ps heating period. Following the heating, equilibrium was established over 3 ps at 300 K using the NVT ensemble. Once the systems were equilibrated, a 4 ps simulation using the microcanonical (NVE) ensemble was performed on each system. The last 3 ps from this simulation were used in further calculations for electronic couplings and energies.

Single point calculations from the structures generated by the MD simulations were performed using the OpenMX software package[37,38] with the PBE functional. The calculations produced the KS orbital energies, wave functions and overlap matrices needed to compute the electronic couplings for electron and hole transfer. The electrostatic potential plots were obtained with the Gaussian software and Multiwfn code post-processing.

3. RESULTS AND DISCUSSION

The simulation cells for both systems consist of two layers of corner sharing $[PbI_6]^{-4}$ units. Each polyhedron interacts with four BZA/F-BZA groups, with their nitrogen tails pointed toward the crystals, as shown in Figure 1a. In the case of the F-BZA spacer, the fluorine atoms are located at the para-position relative to the ammonium ion tail. The layers are categorized by the PbI polyhedron and interacting BZA/F-BZA groups, shown in Figure 1c. The energies of the two layers are approximately equivalent due to symmetry.

In the BZA-PbI_4 system, the charge is contained within the carbon ring. Fluorine substitution migrates this charge density onto the fluorine atom, as visualized in Figure 2a,b. This can create a new channel for charge mobility and transport, potentially increasing the rates of charge transfer between layers. The newly formed transport channel can allow for charges to flow more efficiently as the insulating nature of the organic spacers is weakened. The significant shift in the electron density of the ligand upon the fluorination increases its dipole moment from 1.34 to 3.07 D. The ligands are next to each other, and the dipole moment of the fluorinated ligand points primarily along the C−F bond. Thus, the dipole moments point in the opposite direction, and the dipole−

https://doi.org/10.1021/acsami.4c17876
ACS Appl. Mater. Interfaces 2025, 17, 2032−2040

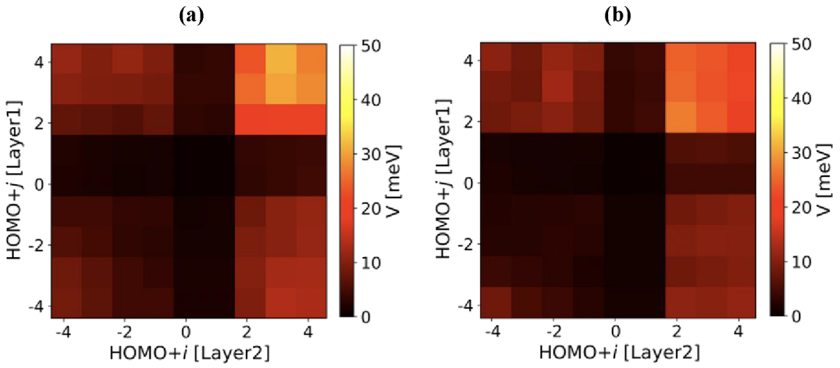

Figure 4. 2D color plots of absolute values of the orbital-resolved electronic coupling between layers in (a) BZA-PbI_4 and (b) F-BZA-PbI_4. The data for both systems are canonically averaged at 300 K.

Table 1. Parameters Required to Calculate the Marcus Charge Transfer Time Scale (τ_{Marcus}) and Charge Carrier Hopping Mobility ($\mu_{hopping}$) for Electrons through LUMO and Holes through HOMO, Including the Root-Mean-Square Electronic Coupling ($\langle V_{kl}^2 \rangle^{1/2}$), the Reorganization Energy (λ), and the Distance between the Layer Center of Masses (L)

		$\langle V_{kl}^2 \rangle^{1/2}$(meV)	λ (eV)	τ_{Marcus}	L (Å)	$\mu_{hopping}$ ($cm^2\ V^{-1}\ s^{-1}$)
non-fluorinated	LUMO	0.442	0.907	1.790 μs	14.073	4.255×10^{-7}
	HOMO	4.261	0.632	1.142 ns		6.668×10^{-4}
fluorinated	LUMO	0.435	0.547	44.812 ns	13.482	1.560×10^{-5}
	HOMO	3.663	0.498	0.377 ns		1.852×10^{-3}

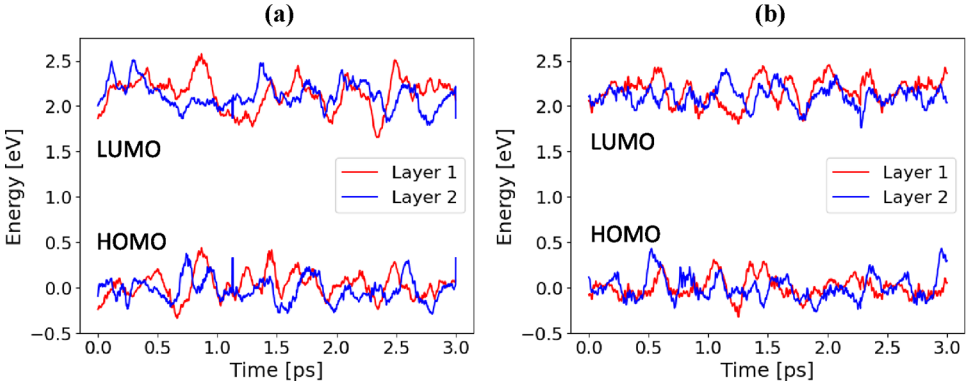

Figure 5. Evolution of the diabatic HOMO and LUMO of the two layers in (a) BZA-PbI_4 and (b) F-BZA-PbI_4 over the final 3 ps of the MD simulation. The HOMO energy averaged over both layers is set to zero for both systems.

dipole interaction is favorable, enhancing interaction between the layers and the system stability.

Parts c and d of Figure 2 show geometries of interacting ligands from different layers in system's optimized geometry. The nonfluorinated system, part c, exhibits $\pi-\pi$ stacking that facilitates interlayer electronic coupling. The ligand geometry changes significantly upon fluorination, part d. The distance between the π-electron systems grows. At the same time, the NH_3 groups rotate in order to allow an H atom to approach the F atom and form an H···F hydrogen bond. As the NH_3 tails to rotate toward the fluorine, the C−C−F angle distorts from 160 degrees in the pristine system to 147 degrees in the fluorinated system. The energy for these significant geometric changes are provided by the created H···F hydrogen bonds. The H···F distance in the fluorinated system is 2.62 Å, while the corresponding H···H distance in the pristine system is 3.45 Å, nearly an angstrom larger. The 2.62 Å H···F distance falls within the 2−3 Å range commonly accepted for H···F bonding.[45,46]

We computed the interlayer interaction energy by subtracting the energy of each layer, in the optimized double-layer geometry, from the total energy of the system, $\Delta E_{int} = E_{total} - (E_{L1} + E_{L2})$. The calculated values are −13.057 eV and −14.160 eV for the BZA and F-BZA systems, respectively. The difference is quite substantial, nearly 10%, given that the systems differ only by substitution of a single H atom for an F atom in the ligands. The quantitative data confirm that the interaction becomes stronger upon the fluorination. Thus, the hydrogen bonding and dipole−dipole interactions between ligands from the opposite layers create a more compact and stable structure in the fluorinated perovskite.

The band structures and pDOS of the respective systems show that in both cases, the band edge states are dominated by contributions from the lead-iodide crystals. More specifically based on the pDOS, in both cases iodine orbitals contribute the most to the valence band maximum, i.e., the highest occupied molecular orbital (HOMO), and lead orbitals contribute the most to the conduction band minimum, i.e.,

https://doi.org/10.1021/acsami.4c17876
ACS Appl. Mater. Interfaces 2025, 17, 2032−2040

Table 2. Canonical Root-Mean-Square Displacements of the Individual Types of Atoms as well as all Atoms of the Organic Spacers and Inorganic Crystal Layers for the BZA and F-BZA Systems

	average displacement (Å)							
	Pb	I	N	H	C	F	organic spacers	inorganic crystals
non-fluorinated	0.71	0.83	1.04	1.46	0.91		1.25	0.81
fluorinated	0.63	0.74	0.86	1.21	0.73	1.01	1.02	0.72

the lowest unoccupied molecular orbital (LUMO). Fluorine does not contribute to band edge states of the overall system, and instead has a peak located 1 eV below the HOMO. Based on the positions of the fluorine contributions, the addition of fluorine also does not contribute to the band edge states of the organic spacers. Fluorine, therefore, is not expected to contribute to the electronic coupling of the donor−acceptor states. This observation raises the question of how fluorination enhances interlayer charge transport if fluorine atoms do not contribute to the electronic coupling directly. The high-symmetry band calculations illustrate that both systems have a direct bandgap of 2.11 eV at the Γ-point, further confirming that fluorine has no effect on the band edge states.

Figure 4 is a two-dimensional representation of the average absolute electronic coupling between layers for both BZA and F-BZA systems around the HOMO and LUMO states. HOMO+j references the j^{th} state in layer one and HOMO+i indicates the i^{th} for layer 2. The average absolute coupling values are given in Table 1 for both HOMO and LUMO. The interlayer couplings are about an order of magnitude larger for holes than electrons, and are larger than those reported in previous work by Li et al.[18] The increase in coupling magnitude of the current system relative to ref.[18] is most likely due to the conjugated benzyl group, which is present in the similar organic semiconductors studied by Giannini et al. which also yield larger electronic coupling values.[47]

Figure 5 illustrates the energy fluctuations of the HOMO and LUMO for both layers at 300 K. The properties of these orbitals are directly related to charge transport, since the HOMO facilitates hole transfer and the LUMO electron transfer. Fluctuations of the orbital energies determine the reorganization energy. Eq. 12, that enters the Marcus rate expression, Eq. 11. The orbital energy fluctuations are reduced by fluorination, resulting in the smaller reorganization energies in Table 1.

The average atomic displacements have been calculated to further validate the conclusions based on Figure 5. The results are summarized in Table 2. The addition of fluorine in the organic spacers decreases the average displacement of the organic spacers by about 18% and the inorganic crystal layers by 11%. This further supports the reduced reorganization energies in the fluorinated systems, Table 1. The fluorine atoms act as a stabilizer by enhancing hydrogen bonding and dipolar interactions between spacers and reducing vibrationally induced fluctuations in the donor and acceptor energies. Fluorine substitution decreases the average displacement for all atom types, indicating that it makes the overall 2D perovskite structure more stable.

The charge transfer rate of the Marcus theory, Eq. 11, depends on two key parameters, the electronic coupling $\langle V^2 \rangle$, Figure 4, and the reorganization energy λ, Figure 5. The dependence on the coupling is quadratic, while the dependence on the organization energy is exponential, i.e., stronger. One could have assumed a priori that the fluorination should enhance the electronic coupling between layers, since the fluorine atom extends the charge density into the interlayer region, Figure 2. However, the pDOS analysis shows that fluorine atoms do not contribute to the band edge states of the organic spacers, Figure 3b inset, and therefore, they should not influence the donor−acceptor coupling directly. Moreover, the data shown in Table 1 demonstrates that fluorination slightly decreases the coupling.

Our analysis demonstrates that the enhancement of the interlayer charge transport by the fluorination stems from the reduced reorganization energies, Table 1. A smaller reorganization energy gives a larger transfer rate, Eq. 11. The reorganization energies show significant variation when fluorine is added to the system, with a 50% difference between the BZA and F-BZA for the electron transfer and a 24% difference for the hole transfer. In comparison, the couplings differ by only 2% and 15%, respectively. Combined with the stronger, exponential dependence of the Marcus rate on the reorganization energy compared to the quadratic coupling dependence, these data demonstrate that the Marcus rates and charge hopping times are influenced much more by the reorganization energies than the electronic couplings.

At the atomistic level, the donor−acceptor coupling depends on overlap of corresponding wave functions. The overlap decreases upon the fluorination, because the distance between the π-electron systems of the ligands from the opposite layers grows to allow formation of the H···F hydrogen bonding, Figure 2d. The donor−acceptor coupling decreases as well, Table 1. The reorganization energy is related to thermal structural fluctuations of the system.[48] The H···F hydrogen bonding stabilizes the system, the increased dipole−dipole interaction between the ligands provides further stabilization. The tighter structure of the fluorinated system decreases structural fluctuations, Table 2, thereby reducing the reorganization energy, and making the charge transfer faster, Table 1.

The donor−acceptor couplings for hole and electron transfer differ by an order of magnitude, as summarized in Table 1, contributing strongly to the faster transport of holes than electrons. The smaller reorganization energies for holes than electrons contribute to the faster hole transport as well. The hole transfer rate is 3 orders of magnitude larger than the electron transfer rate in the BZA system. The difference is 2 orders of magnitude in the F-BZA system. Fluorine substitution significantly improves both electron and hole hopping, assisting in increasing efficiencies of 2D perovskite solar cells.

The importance of position of the fluorine substituent in F-BZA was discussed by Yan et al.[30] who showed that fluorine substitution in the para- position gives the best efficiency, compared to the meta- and ortho- positions. Our results show that placing F in the meta- or ortho- positions puts it too far from the -NH_3 group, preventing the hydrogen bonding. Additionally, placing F in the meta- and ortho- positions creates smaller ligand dipole moments compared to the para-

https://doi.org/10.1021/acsami.4c17876
ACS Appl. Mater. Interfaces 2025, 17, 2032−2040

position. Thus, the para- position is most favorable for stabilizing the system and enhancing the charge transport.

The current work focused on 2D perovskites with a single PbI_6 octahedron across each layer. It is interesting to consider how the organic spacer fluorination may influence the interlayer charge transport for 2D perovskites with thicker inorganic layers. The calculations show that the enhancement of the charge transfer rate is associated with the decreased reorganization energy of the Marcus theory, Table 1. The reorganization energy is decreased because the system becomes more stable structurally, and exhibits reduced atomic fluctuations upon the fluorination, Table 2. The charges are localized on the inorganic layers, and therefore, reorganization of the inorganic layers is the most important. The spacer fluorination stabilizes the overall structure, however, the influence of the spacers on the properties of the inorganic layers should decrease with increasing layer thickness. The influence of the spacer fluorination on the reorganization energy will be stronger if charges are localized toward the layer surface. Therefore, one can expect that the influence of the organic spacer fluorination on the charge transport across the layers should decrease with increasing layer thickness. Since the spacer fluorination decreases the donor−acceptor coupling, Table 1, one can envision a situation in which changes in the coupling outweigh changes in the reorganization energy, and the fluorination decreases charge mobility.

4. CONCLUSIONS

2D perovskites are a promising alternative to conventional 3D perovskites due to their higher stability and tunable bandgaps. However, 2D perovskites struggle with efficient charge transport due to inert organic spacers that isolate charges into separate lead-halide layers. Fluorine substitution in the para-position of the benzene ring in the BZA organic spacer has shown to be an effective strategy for improving the charge transfer rates and charge mobility. We have performed a comprehensive ab initio simulation combining the POD method, MD modeling, and Marcus theory calculations to elucidate the origin of this effect. Perhaps unexpectedly, our simulations have shown that the main reason for the enhancement in the charge mobility stems from stabilization of the overall organic−inorganic structure rather than increased interlayer electronic coupling. It may be expected a priori that migration of charge density to the highly electronegative fluorine atoms should help to facilitate overlap of donor and acceptor electron densities, and thus increase the electronic coupling. However, the fluorine atom does not contribute to the ligand frontier orbitals that are responsible for the donor−acceptor interaction. Fluorination does bring the layers closer together, which increases overlap of layer wave functions. However, the main factor is the improved stability of the overall system. By enhancing hydrogen bonding and dipolar interactions, fluorination makes the F-BZA system more robust, reducing atomic fluctuations. As a result, the reorganization energy entering the Marcus rate expression is decreased, and the charge transfer rate increases. The difference in the electronic donor−acceptor coupling facilitated by the HOMO and LUMO explains the significant difference in the hole and electron mobilities seen in these systems. The difference in the reorganization energies is an important factor in this case as well. The calculated electron and hole mobilities are enhanced by 1−2 orders of magnitude after the fluorination, in agreement with recent experiments. The simulations generate detailed atomistic insights into charge transfer across layers in 2D lead-halide perovskites, providing important practical guidelines. Tuning organic spacers to make the system more robust simultaneously improves chemical stability and charge transport.

AUTHOR INFORMATION

Corresponding Author

Oleg V. Prezhdo − *Department of Chemistry and Department of Physics and Astronomy, University of Southern California, Los Angeles, California 90089, United States;* orcid.org/0000-0002-5140-7500; Email: prezhdo@usc.edu

Authors

Elizabeth Stippell − *Department of Chemistry, University of Southern California, Los Angeles, California 90089, United States*

Wei Li − *School of Chemistry and Materials Science, Hunan Agricultural University, Changsha 410128, PR China;* orcid.org/0000-0002-9999-5081

Claudio Quarti − *Laboratory for Chemistry of Novel Materials, University of Mons, Mons 7000, Belgium;* orcid.org/0000-0002-5488-1216

David Beljonne − *Laboratory for Chemistry of Novel Materials, University of Mons, Mons 7000, Belgium;* orcid.org/0000-0002-2989-3557

Complete contact information is available at: https://pubs.acs.org/10.1021/acsami.4c17876

Notes

The authors declare no competing financial interest.

ACKNOWLEDGMENTS

The research was supported by funding from the US Department of Energy, grant DE-SC0014429. W. L. acknowledges financial support of National Natural Science Foundation of China, grant no. 22373033. D.B. is a research director and C.Q. a research associate of the Belgian Fund for Scientific Research FNRS.

REFERENCES

(1) Mao, L.; Stoumpos, C. C.; Kanatzidis, M. G. Two-Dimensional Hybrid Halide Perovskites: Principles and Promises. *J. Am. Chem. Soc.* **2019**, *141*, 1171−1190.

(2) Xiang, W. J.; Cronk, E.; Wall, J.; Li, L.; Zhu, K.; Berry, J. J.; Lad, R. J.; Yu, L. P.; Yan, F. Double Perovskite Interlayer Stabilized Highly Efficient Perovskite Solar Cells. *ACS Appl. Mater. Interfaces* **2024**, *16*, 44988−44996.

(3) Yadav, A.; Ahmad, S. Single Crystal Ruddlesden-Popper and Dion-Jacobson Metal Halide Perovskites for Visible Light Photodetectors: Present Status and Future Perspectives. *ACS Appl. Mater. Interfaces* **2024**, *16*, 43134−43155.

(4) Leung, T. L.; Ahmad, I.; Syed, A. A.; Ng, A. M. C.; Popović, J.; Djurišić, A. B. Stability of 2d and Quasi-2d Perovskite Materials and Devices. *Commun. Mater.* **2022**, *3*, 63.

(5) Jiang, W.; Li, H.; Xing, Z.; Zhao, Y.; Liu, D.; Di, H.; Zhao, C.; Liu, Y.; Zhao, Y. PEAI Surface Treatment for Low Ion Migration and High-Performance $FAPbBr_3$ Single-Crystal X-ray Detectors. *ACS Appl. Mater. Interfaces* **2024**, *16*, 51630−51638.

(6) Park, J.; Kim, J.; Yun, H.-S.; Paik, M. J.; Noh, E.; Mun, H. J.; Kim, M. G.; Shin, T. J.; Seok, S. I. Controlled Growth of Perovskite Layers with Volatile Alkylammonium Chlorides. *Nature* **2023**, *616*, 724−730.

(7) Stanton, R.; Trivedi, D. J. Atomistic Description of the Impact of Spacer Selection on Two-Dimensional (2d) Perovskites: A Case

Study of 2d Ruddlesden-Popper $CsPbI_3$ Analogues. *J. Phys. Chem. Lett.* **2022**, *13*, 12090−12098.
(8) Wang, Z.; Liu, X.; Ren, H.; Liu, L.; Tang, X.; Yao, X.; Su, Z.; Gao, X.; Wei, Q.; Xie, H.; Zheng, Y.; Li, M. Insight into the Enhanced Charge Transport in Quasi-2d Perovskite Via Fluorination of Ammonium Cations for Photovoltaic Applications. *ACS Appl. Mater. Interfaces* **2022**, *14*, 7917−7925.
(9) Li, X.; Hoffman, J. M.; Kanatzidis, M. G. The 2d Halide Perovskite Rulebook: How the Spacer Influences Everything from the Structure to Optoelectronic Device Efficiency. *Chem. Rev.* **2021**, *121*, 2230−2291.
(10) García-Benito, I.; Quarti, C.; Queloz, V. I. E.; Hofstetter, Y. J.; Becker-Koch, D.; Caprioglio, P.; Neher, D.; Orlandi, S.; Cavazzini, M.; Pozzi, G.; Even, J.; Nazeeruddin, M. K.; Vaynzof, Y.; Grancini, G. Fluorination of Organic Spacer Impacts on the Structural and Optical Response of 2d Perovskites. *Front. Chem.* **2020**, *7*, 946.
(11) Lei, Y.; Li, Z.; Wang, H.; Wang, Q.; Peng, G.; Xu, Y.; Zhang, H.; Wang, G.; Ding, L.; Jin, Z. Manipulate Energy Transport Via Fluorinated Spacers Towards Record-Efficiency 2d Dion-Jacobson $CsPbI_3$ Solar Cells. *Science Bulletin* **2022**, *67*, 1352−1361.
(12) Zhang, F.; Kim, D. H.; Lu, H.; Park, J.-S.; Larson, B. W.; Hu, J.; Gao, L.; Xiao, C.; Reid, O. G.; Chen, X.; Zhao, Q.; Ndione, P. F.; Berry, J. J.; You, W.; Walsh, A.; Beard, M. C.; Zhu, K. Enhanced Charge Transport in 2d Perovskites Via Fluorination of Organic Cation. *J. Am. Chem. Soc.* **2019**, *141*, 5972−5979.
(13) Byeon, J.; Cho, S. H.; Jiang, J.; Jang, J.; Katan, C.; Even, J.; Xi, J.; Choi, M.; Lee, Y. S. Structural Isomer of Fluorinated Ruddlesden-Popper Perovskites toward Efficient and Stable 2d/3d Perovskite Solar Cells. *ACS Appl. Mater. Interfaces* **2023**, *15*, 27853−27864.
(14) Li, Q.; Dong, Y.; Lv, G.; Liu, T.; Lu, D.; Zheng, N.; Dong, X.; Xu, Z.; Xie, Z.; Liu, Y. Fluorinated Aromatic Formamidinium Spacers Boost Efficiency of Layered Ruddlesden−Popper Perovskite Solar Cells. *ACS Energy Letters* **2021**, *6*, 2072−2080.
(15) Zhang, H.; Wang, R.; Yang, L.; Hu, Z.; Liu, H.; Liu, Y. Modulating the Dipole Moment of Secondary Ammonium Spacers for Efficient 2d Ruddlesden-Popper Perovskite Solar Cells. *Angew. Chem., Int. Ed.* **2024**, *63*, No. e202318206.
(16) Chen, M.; Dong, X.; Xin, Y.; Gao, Y.; Fu, Q.; Wang, R.; Xu, Z.; Chen, Y.; Liu, Y. Crystal Growth Regulation of Ruddlesden−Popper Perovskites Via Self-Assembly of Semiconductor Spacers for Efficient Solar Cells. *Angew. Chem., Int. Ed.* **2024**, *63*, No. e202315943.
(17) Boeije, Y.; Van Gompel, W. T. M.; Zhang, Y.; Ghosh, P.; Zelewski, S. J.; Maufort, A.; Roose, B.; Ooi, Z. Y.; Chowdhury, R.; Devroey, I.; Lenaers, S.; Tew, A.; Dai, L.; Dey, K.; Salway, H.; Friend, R. H.; Sirringhaus, H.; Lutsen, L.; Vanderzande, D.; Rao, A.; Stranks, S. D. Tailoring Interlayer Charge Transfer Dynamics in 2d Perovskites with Electroactive Spacer Molecules. *J. Am. Chem. Soc.* **2023**, *145*, 21330−21343.
(18) Li, W.; Giannini, S.; Quarti, C.; Hou, Z.; Prezhdo, O. V.; Beljonne, D. Interlayer Charge Transport in 2d Lead Halide Perovskites from First Principles. *J. Chem. Theory Comput.* **2023**, *19*, 9403−9415.
(19) Stanton, R.; Gupta, S. K.; Trivedi, D. J. Probing Strain-Induced Effects on Performance of Low-Dimensional Hybrid Perovskites for Solar Energy Harvesting. *ACS Appl. Mater. Interfaces* **2022**, *14*, 34603.
(20) Hoffman, J. M.; Che, X.; Sidhik, S.; Li, X.; Hadar, I.; Blancon, J.-C.; Yamaguchi, H.; Kepenekian, M.; Katan, C.; Even, J.; Stoumpos, C. C.; Mohite, A. D.; Kanatzidis, M. G. From 2d to 1d Electronic Dimensionality in Halide Perovskites with Stepped and Flat Layers Using Propylammonium as a Spacer. *J. Am. Chem. Soc.* **2019**, *141*, 10661−10676.
(21) Liu, Y.; Gao, Z.; Tan, Y.; Chen, F. Enhancement of out-of-Plane Charge Transport in a Vertically Stacked Two-Dimensional Heterostructure Using Point Defects. *ACS Nano* **2018**, *12*, 10529−10536.
(22) Zhao, X.; Ball, M. L.; Kakekhani, A.; Liu, T.; Rappe, A. M.; Loo, Y.-L. A Charge Transfer Framework That Describes Supramolecular Interactions Governing Structure and Properties of 2d Perovskites. *Nat. Commun.* **2022**, *13*, 3970.
(23) Nayak, P. K.; Ghosh, D. Tuning Charge Carrier Dynamics through Spacer Cation Functionalization in Layered Halide Perovskites: An Ab Initio Quantum Dynamics Study. *Journal of Materials Chemistry C* **2023**, *11*, 3521−3532.
(24) Li, W.; She, Y.; Vasenko, A. S.; Prezhdo, O. V. Ab initio nonadiabatic molecular dynamics of charge carriers in metal halide perovskites. *Nanoscale* **2021**, *13*, 10239−10265.
(25) Shi, R.; Long, R.; Fang, W. H.; Prezhdo, O. V. Rapid Interlayer Charge Separation and Extended Carrier Lifetimes Due to Spontaneous Symmetry Breaking in Organic and Mixed Organic-Inorganic Dion-Jacobson Perovskites. *J. Am. Chem. Soc.* **2023**, *145*, 5297−5309.
(26) De, A.; Mora Perez, C.; Liang, A.; Wang, K.; Dou, L.; Prezhdo, O.; Huang, L. Tunneling-Driven Marcus-Inverted Triplet Energy Transfer in a Two-Dimensional Perovskite. *J. Am. Chem. Soc.* **2024**, *146*, 4260−4269.
(27) Ma, X.; Fang, W. H.; Long, R.; Prezhdo, O. V. Compression of Organic Molecules Coupled with Hydrogen Bonding Extends the Charge Carrier Lifetime in BA 2 SnI 4. *J. Am. Chem. Soc.* **2024**, *146*, 16314−16323.
(28) Dai, D.; Agrawal, S.; Prezhdo, O. V.; Long, R. Impact of large A-site cations on electron−vibrational interactions in 2D halide perovskites: Ab initio quantum dynamics. *J. Chem. Phys.* **2024**, *160*, 114704.
(29) Jin, L.; Mora Perez, C.; Gao, Y.; Ma, K.; Park, J. Y.; Li, S.; Guo, P.; Dou, L.; Prezhdo, O.; Huang, L. Superior Phonon-Limited Exciton Mobility in Lead-Free Two-Dimensional Perovskites. *Nano Lett.* **2024**, *24*, 3638−3646.
(30) Yan, G.; Sui, G.; Chen, W.; Su, K.; Feng, Y.; Zhang, B. Selectively Fluorinated Benzylammonium-Based Spacer Cation Enables Graded Quasi-2d Perovskites for Efficient and Stable Solar Cells. *Chem. Mater.* **2022**, *34*, 3346−3356.
(31) Lai, X.; Li, W.; Gu, X.; Chen, H.; Zhang, Y.; Li, G.; Zhang, R.; Fan, D.; He, F.; Zheng, N.; Yu, J.; Chen, R.; Kyaw, A. K. K.; Sun, X. W. High-Performance Quasi-2d Perovskite Solar Cells with Power Conversion Efficiency over 20% Fabricated in Humidity-Controlled Ambient Air. *Chemical Engineering Journal* **2022**, *427*, No. 130949.
(32) Ghoreishi, F. S.; Ahmadi, V.; Alidaei, M.; Arabpour Roghabadi, F.; Samadpour, M.; Poursalehi, R.; Johansson, E. M. J. Enhancing the Efficiency and Stability of Perovskite Solar Cells Based on Moisture-Resistant Dopant Free Hole Transport Materials by Using a 2d-Ba_2PbI_4 Interfacial Layer. *Phys. Chem. Chem. Phys.* **2022**, *24*, 1675−1684.
(33) Kondov, I.; Čížek, M.; Benesch, C.; Wang, H.; Thoss, M. Quantum Dynamics of Photoinduced Electron-Transfer Reactions in Dye−Semiconductor Systems: First-Principles Description and Application to Coumarin 343−TiO_2. *J. Phys. Chem. C* **2007**, *111*, 11970−11981.
(34) Ghan, S.; Kunkel, C.; Reuter, K.; Oberhofer, H. Improved Projection-Operator Diabatization Schemes for the Calculation of Electronic Coupling Values. *J. Chem. Theory Comput.* **2020**, *16*, 7431−7443.
(35) Futera, Z.; Blumberger, J. Electronic Couplings for Charge Transfer across Molecule/Metal and Molecule/Semiconductor Interfaces: Performance of the Projector Operator-Based Diabatization Approach. *J. Phys. Chem. C* **2017**, *121*, 19677−19689.
(36) Ghan, S.; Diesen, E.; Kunkel, C.; Reuter, K.; Oberhofer, H. Interpreting Ultrafast Electron Transfer on Surfaces with a Converged First-Principles Newns−Anderson Chemisorption Function. *J. Chem. Phys.* **2023**, *158*, No. 234103.
(37) Ozaki, T. Variationally Optimized Atomic Orbitals for Large-Scale Electronic Structures. *Phys. Rev. B* **2003**, *67*, No. 155108.
(38) Ozaki, T.; Kino, H. Numerical Atomic Basis Orbitals from H to Kr. *Phys. Rev. B* **2004**, *69*, No. 195113.
(39) Löwdin, P. O. On the Non-Orthogonality Problem Connected with the Use of Atomic Wave Functions in the Theory of Molecules and Crystals. *J. Chem. Phys.* **1950**, *18*, 365−375.
(40) Mayer, I. On Löwdin's Method of Symmetric Orthogonalization*. *Int. J. Quantum Chem.* **2002**, *90*, 63−65.

https://doi.org/10.1021/acsami.4c17876
ACS Appl. Mater. Interfaces 2025, 17, 2032−2040

(41) Marcus, R. A. On the Theory of Chemiluminescent Electron-Transfer Reactions. *J. Chem. Phys.* **1965**, *43*, 2654−2657.
(42) Kresse, G.; Hafner, J. Ab Initio Molecular Dynamics for Liquid Metals. *Phys. Rev. B* **1993**, *47*, 558−561.
(43) Perdew, J. P.; Burke, K.; Ernzerhof, M. Generalized Gradient Approximation Made Simple. *Phys. Rev. Lett.* **1996**, *77*, 3865−3868.
(44) Grimme, S.; Antony, J.; Ehrlich, S.; Krieg, H. A Consistent and Accurate Ab Initio Parametrization of Density Functional Dispersion Correction (DFT-D) for the 94 Elements H-Pu. *J. Chem. Phys.* **2010**, *132*, No. 154104.
(45) Safferthal, M.; Greis, K.; Chang, R.; Kirschbaum, C.; Hoffmann, W.; Meijer, G.; von Helden, G.; Pagel, K. Cryogenic infrared spectroscopy reveals remarkably short NH^+ ···F hydrogen bonds in fluorinated phenylalanines. *Phys. Chem. Chem. Phys.* **2023**, *25*, 24783−24788.
(46) Schneider, H. J. Hydrogen Bonds with Fluorine. Studies in Solution, in Gas Phase and by Computations, Conflicting Conclusions from Crystallographic Analyses. *Chemical Science* **2012**, *3*, 1381−1394.
(47) Giannini, S.; Carof, A.; Ellis, M.; Yang, H.; Ziogos, O. G.; Ghosh, S.; Blumberger, J. Quantum Localization and Delocalization of Charge Carriers in Organic Semiconducting Crystals. *Nat. Commun.* **2019**, *10*, 3843.
(48) Kamisaka, H.; Kilina, S. V.; Yamashita, K.; Prezhdo, O. V. Ultrafast Vibrationally-Induced Dephasing of Electronic Excitations in Pbse Quantum Dot. *Nano Lett.* **2006**, *6*, 2295−2300.

https://doi.org/10.1021/acsami.4c17876
ACS Appl. Mater. Interfaces 2025, 17, 2032−2040